International Journal of Latest Research in Engineering and Technology (IJLRET)
ISSN: 2454-5031
www.ijlret.com || Volume 11 - Issue 08 || August 2025 || PP. 51-57

Dynamic Performance Comparison of Speed and Position Estimators in Sensorless IPMSM Drives

Dr. Dongwoo Lee[1]
[1]*Assistant Professor, Department of Electrical & Control Engineering, Cheongju University, Korea*

Abstract: This study investigates a study of the estimator performance of a position sensorless control based on backelectromotive force (back-EMF) estimation in an interior permanent magnet synchronous motor (IPMSM). The characteristic of the estimated back-EMF signals is analyzed using various mathematical models of the IPMSM. Sensorless control based on the extended electromotive force (EMF) model in the rotor reference frame incorporates a back-EMF estimator, such as a disturbance observer, and a rotor position estimator, which may be implemented using either a phaselocked loop (PLL) or a Luenberger observer (LO). To compare the transient performance of rotor position estimators, the design and gain selection methods of estimators are introduced. And, the effect of current sensor error has been figured out that the estimated speed error and position error are directly affected. The feasibility of the introduced estimator and current error effect are verified through simulation results.

Keywords: IPMSM, sensorless control, speed and position estimator

1. Introduction

Permanent Magnet Synchronous Motors (PMSMs) have become prevalent in precision control applications, attributed to their compact structure and high conversion efficiency. The literature highlights IPMSMs as a promising topology, owing to their ability to achieve high torque through the synergistic effect of magnetic and reluctance torque [1]. Sensorless control techniques for PMSMs have also gained popularity, offering advantages such as enhanced reliability, reduced system cost, and simplified mechanical design.

Achieving high-performance sensorless control requires accurate estimation of rotor position and speed. Two primary approaches are commonly used for this purpose. one relies on the back-EMF generated during motor operation to facilitate sensorless control [2], while the other utilizes high-frequency voltage injection, extracting rotor position information from the resulting current response of motor [3].

Various methods, including state observer-based approaches, have been proposed for estimating the back-EMF in permanent magnet synchronous motors (PMSMs), utilizing an extended EMF mathematical model formulated in the rotor reference frame[2],[6]. And, several estimators, including phaselocked loop (PLL)based and Luenberger observer (LO)based methods, have been proposed to extract the estimated rotor speed and position from the amplitude of the back-EMF.[9]. However, the analysis at low-speed operation is not addressed, and the investigation of stable observer gain under load torque variation remains either insufficient or overly complex. In addition, the low overshoot characteristic of the estimated speed error during torque transients has not been adequately considered. Although the effects of current measurement errors on rotor position estimation have been studied for stable sensorless control, their impact during transient conditions has received limited attention[2-13].

In this paper, the sensorless control with position estimators is studied in based on the extended EMF model in the rotor reference frame for fast response in transient state and high speed. And the PLL-type estimator, PLL-type estimator with double integral term and LO-type estimator are used to compare the performance of estimated rotor speed and position. To compare the stability on designed estimators in the transient state, the simulation results are analyzed with various conditions.

2. Mathematical model of IPMSMs

Fig. 1 shows a space vector diagram for a PMSM [5]. The α–β axes correspond to the stationary reference frame, whereas the d–q axes represent the rotor reference frame. The γ-δ axis is an estimated frame used in vector control for sensorless.The IPMSMs voltage equation in the d-q axis can be described through the following:

$$\begin{bmatrix} V_d \\ V_q \end{bmatrix} = \begin{bmatrix} R + pL_d & -\omega_r L_q \\ \omega_r L_d & R + pL_q \end{bmatrix} \cdot \begin{bmatrix} i_d \\ i_q \end{bmatrix} + \begin{bmatrix} 0 \\ \omega_r \phi_m \end{bmatrix} \quad (1)$$

International Journal of Latest Research in Engineering and Technology (IJLRET)
ISSN: 2454-5031
www.ijlret.com || Volume 11 - Issue 08 || August 2025 || PP. 51-57

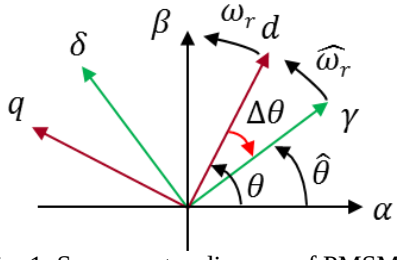

Fig. 1: Space vector diagram of PMSM.

To simplify the analytical modeling of the interior permanent magnet synchronous motor (IPMSM), the extended electromotive force (EMF) formulation can be incorporated into the rotor reference frame as follows:

$$\begin{bmatrix} V_\gamma \\ V_\delta \end{bmatrix} = \begin{bmatrix} R + pL_d & -\omega_r L_q \\ \omega_r L_q & R + pL_d \end{bmatrix} \cdot \begin{bmatrix} i_\gamma \\ i_\delta \end{bmatrix} + \omega_r \lambda_{PM} \begin{bmatrix} -\sin \Delta\theta \\ \cos \Delta\theta \end{bmatrix} + (\hat{\omega}_r - \omega_r) L_d \begin{bmatrix} -i_\delta \\ i_\gamma \end{bmatrix} \quad (2)$$

The estimated rotor position error$\Delta\hat{\theta}$can be calculated using (3):

$$\Delta\hat{\theta} = tan^{-1}\left(\frac{-E_{ex} \cdot sin\ \Delta\theta}{E_{ex} \cdot cos\ \Delta\theta}\right) = -\tan^{-1}\left(\frac{\hat{e}_\gamma}{\hat{e}_\delta}\right) \quad (3)$$

3. Extended EMF Estimation

The equivalent block diagram of disturbance observer for the estimation of extended EMF of γ-axis is shown in Fig. 2. The g_{ob} is the bandwidth of the disturbance observer. The disturbance observer incorporates a differential operator to derive the inverse model of the system. To mitigate the adverse effects associated with differentiation, the observer integrates both a low-pass filter and a high-pass filter, as illustrated in (4). Therefore, the appropriate selection of the observer gain is crucial for enhancing transient stability in sensorless control systems [2].

$$\hat{\vec{E}}_{\gamma\delta} = \frac{g_{ob}}{s+g_{ob}}\left(\vec{V}^*_{\gamma\delta} + j\hat{\omega}_r \bar{L}_q \cdot \vec{I}_{\gamma\delta} - \bar{R} \cdot \vec{I}_{\gamma\delta}\right) - \frac{s}{s+g_{ob}}\left(\bar{L}_d \cdot g_{ob} \cdot \vec{I}_{\gamma\delta}\right) \quad (4)$$

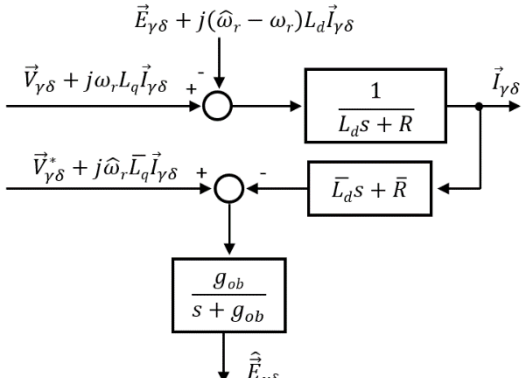

Fig. 2: Equivalent block diagram for the extended EMF estimation.

The parameter g_{ob} can be decided by manual tuning for robust estimation. It is also noteworthy that the bandwidth of the current control loop is significantly higher than that of the speed control loop, which reflects the hierarchical structure of the motor control system. Consequently, the observer filter bandwidth must be sufficiently large to ensure accurate state estimation and maintain system stability.In general, the g_{ob} is defined as two times of ω_r.In this paper, it is set as g_{ob} = 1000 rad/s.

4. Speed and position estimation

4.1 Analysis of PLL-type Estimator

Regarding the stable bandwidth selection of PLL-type estimator, Reference [4] outlines foundational principles for bandwidth tuning method.In Fig. 3, the PLL-type estimator consists of PI regulator, low pass filter and integral term to generate $\hat{\theta}$ and $\hat{\omega}_r$. In general, the $\hat{\omega}_o$ in Fig. 4 or the output of the integral term in the PI regulator is utilized as the estimated rotor speed for both motor control and extended back-EMF estimation.

Meanwhile, the filtered estimated speed $\hat{\omega}_r$ is employed to suppress undesirable noise effects in the current control loop, particularly under nonsinusoidal back-EMF conditions [2], [10].

These estimated values are transformed through reference frame conversion to ensure synchronism between the γ–δ frame and the d–q frame. From (5) with Fig. 3, the estimated rotor angular speed $\hat{\omega}_r$ is defined as (6).

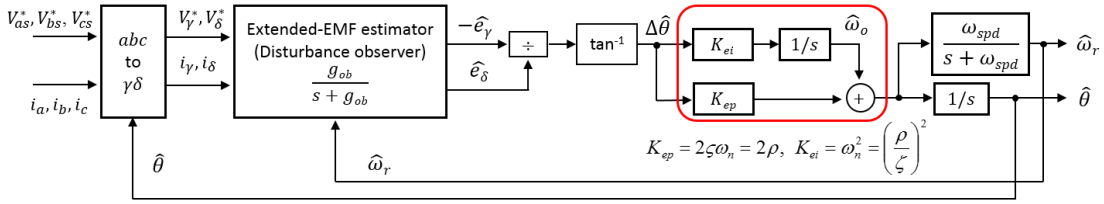

Fig. 3: Block diagram of the PLL-type estimator for sensorless control

$$\hat{\theta} = \frac{K_{ep}\cdot s+K_{ei}}{s^2+K_{ep}\cdot s+K_{ei}}\cdot\theta \quad (5)$$

$$\hat{\omega}_r = \left(K_{ep}+\frac{K_{ei}}{s}\right)\cdot\left(\frac{g_{ob}}{s+g_{ob}}\right)\cdot\left(\frac{\omega_{spd}}{s+\omega_{spd}}\right)\cdot\Delta\hat{\theta} \approx \left(K_{ep}+\frac{K_{ei}}{s}\right)\cdot\left(\frac{g_{ob}}{s+g_{ob}}\right)\cdot\left(\frac{\omega_{spd}}{s+\omega_{spd}}\right)\cdot(\theta-\hat{\theta}) \quad (6)$$

If $\hat{\theta}$ in (5) is inserted into (6) and the g_{ob} is defined as 5 times of PLL-type estimator bandwidth to ignore the effect of g_{ob}, the $\hat{\omega}_r$ can be rearranged into

$$\hat{\omega}_r \approx \left(K_{ep}+\frac{K_{ei}}{s}\right)\cdot\left(\frac{\omega_{spd}}{s+\omega_{spd}}\right)\cdot\left(\frac{s^2}{s^2+K_{ep}\cdot s+K_{ei}}\right)\cdot\theta = \left(\frac{\omega_{spd}}{s+\omega_{spd}}\right)\cdot\left(\frac{K_{ep}\cdot s+K_{ei}}{s^2+K_{ep}\cdot s+K_{ei}}\right)\cdot\omega_r \quad (7)$$

To analyze the transfer function of PLL-type estimator in (7), the 3rd order characteristic equation is derived, as shownin (8)

$$c(s) = (s+\omega_{spd})(s^2+K_{ep}\cdot s+K_{ei}) = (s+\omega_{spd})(s^2+2\varsigma\omega_n s+\omega_n^2) \quad (8)$$

$$\therefore K_{ep} = 2\varsigma\omega_n, K_{ei} = \omega_n^2 \quad (9)$$

Here, ζ denotes the damping ratio and ω_n represents the natural frequency. Accordingly, the tracking performance of the PLL-type estimator is governed by ζ and ω_n, which must be properly selected to ensure optimal behavior. When ζ = 1, the system exhibits non-oscillatory and critically damped behavior, with both poles located at -ρ, resulting in stable dynamics. The dynamic response of the PLL-type estimator is primarily characterized by the natural frequency ω_n. Furthermore, the speed estimation value ω_{spd} can be defined through simulation-based evaluation after setting the parameter ρ.

4.2 PLL-type Estimator Design with aDouble Integral Term

The PLL-type estimator with a double integral term shows in Fig. 4. When $\Delta\hat{\theta} \approx \Delta\theta = \theta - \hat{\theta}$ is assumed, (10) can be derived from Fig. 4.

$$\hat{\theta} = \frac{K_2\cdot s^2+K_1\cdot s+K_3}{s^3+K_2\cdot s^2+K_1\cdot s+K_3}\cdot\theta \quad (10)$$

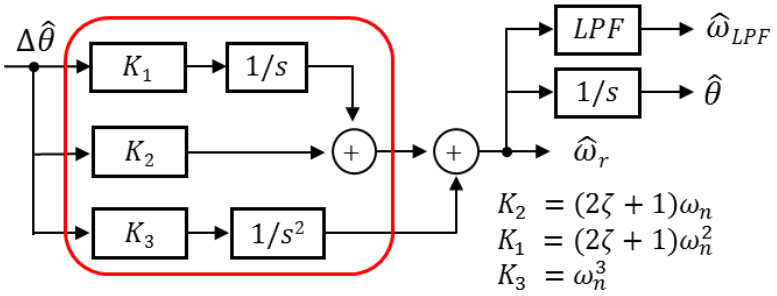

Fig. 4: Block diagram of the PLL-type estimator with a double integral term.

where K1, K2 and K3 are gains for PLL-type estimator. $\hat{\omega}_r$ is derived as (11)

$$\hat{\omega}_r = \left(\frac{K_1}{s} + K_2 + \frac{K_3}{s^2}\right) \cdot \Delta\hat{\theta} \approx \left(\frac{K_1}{s} + K_2 + \frac{K_3}{s^2}\right) \cdot \left(\theta - \hat{\theta}\right) \quad (11)$$

If $\hat{\theta}$ in (10) is inserted into (11), it can be defined into (12).

$$\hat{\omega}_r = \frac{K_2 \cdot s^2 + K_1 \cdot s + K_3}{s^3 + K_2 \cdot s^2 + K_1 \cdot s + K_3} \cdot \omega_r \quad (12)$$

The estimator gains can be set according to the following condition

$$s^3 + K_2 s^2 + K_1 s + K_3 = (s + \omega_n)(s^2 + 2\varsigma\omega_n \cdot s + \omega_n^2)$$
$$\therefore K_1 = (2\varsigma + 1)\omega_n^2, K_2 = (2\varsigma + 1)\omega_n^2, K_3 = \omega_n^3 \quad (13)$$

4.3 Luenberger Observer (LO) type estimator

TheLO-type estimator with a double integral term shows in Fig. 5. When $\Delta\hat{\theta} \approx \Delta\theta = \theta - \hat{\theta}$ is assumed, (14) can be derived from Fig. 5

$$\hat{\theta} = \frac{J \cdot s^3 + (B + \hat{J}_m K_{ed}) s^2 + (\hat{B}_m K_{ed} + K_{ep}) s + K_{ei}}{\hat{J}_m \cdot s^3 + (\hat{B}_m + \hat{J}_m K_{ed}) s^2 + (\hat{B}_m K_{ed} + K_{ep}) \cdot s + K_{ei}} \quad (14)$$

where K_{ep}, K_{ei} and K_{ed} are gains for LO type estimator. From the characteristic equation of (14), the gains of estimator can be selected with the same roots as the followings

$$K_{ep} = 3\beta^2 \cdot J, \; K_{ei} = \beta^3 \cdot J, \; K_{ed} = -3\beta \quad (15)$$

where β is the triple root of the characteristic equation for the stable control system.

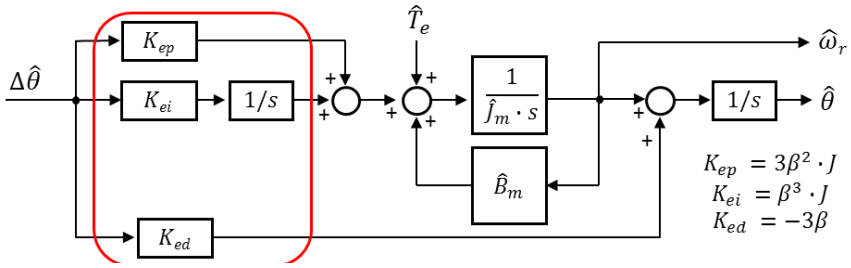

Fig. 5: LO type estimator including torque feed-forward.

5. Simulation results

The configuration of the simulation system is illustrated in Fig. 6. The PLL-type estimator calculates the rotor position and speed based on the observed back-EMF signals. To validate the accuracy of the estimated information, the results are compared with actual rotor angle and speed obtained from resolver output signals.The sensorless control strategy for IPMSMs was implemented and validated through PSIM simulations. The sensorless control architecture is illustrated in Figure 6. Also, IPMSM parameters is listed in Table 1.

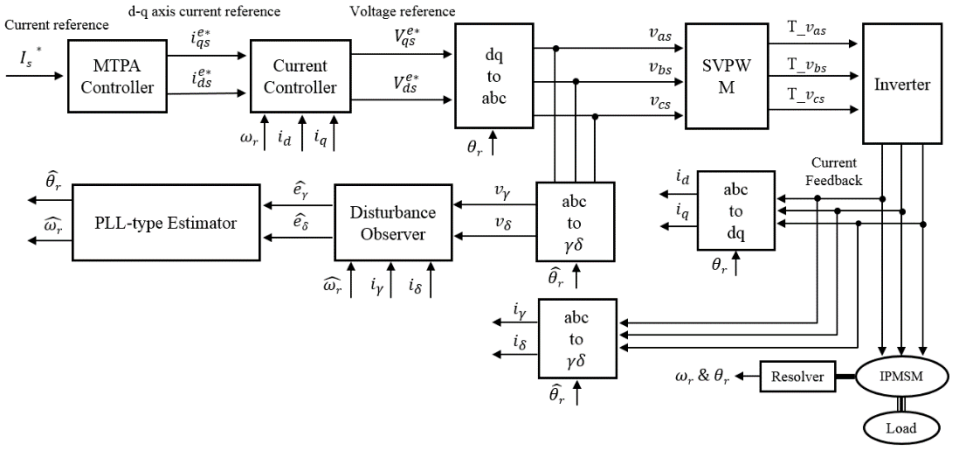

Fig. 6: Functional block diagram of the sensorless control included PLL-type estimator for simulation.

Table 1: IPMSM parameters

Parameter	Value
Number of poles	4
Rated Speed	1500 [r/mim]
Stator resistance	0.814 [Ω]
d-axis Inductance	10.7 [mH]
q-axis Inductance	26.3 [mH]
Back-EMF constant	0.14693 [V•s/rad]
Rotor inertia	0.001641 [kg-m^2]
Rated torque	1.8 [Nm]

The performance of estimators on position and speed estimation and the maximum overshoot of estimated speed and position error are compared under step torque variation and rampwise speed variation by PSIM simulation such as Fig.7, Fig. 8 and Fig. 9.

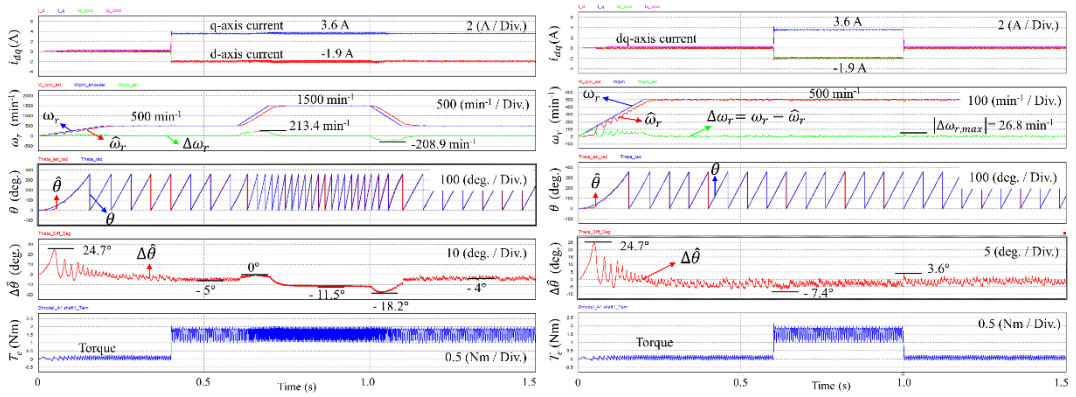

(a)(b)

Fig. 7: Simulation results on PLL-type estimator (a)Maximum overshoot in speed variation (b)Maximum overshoot in torque variation.

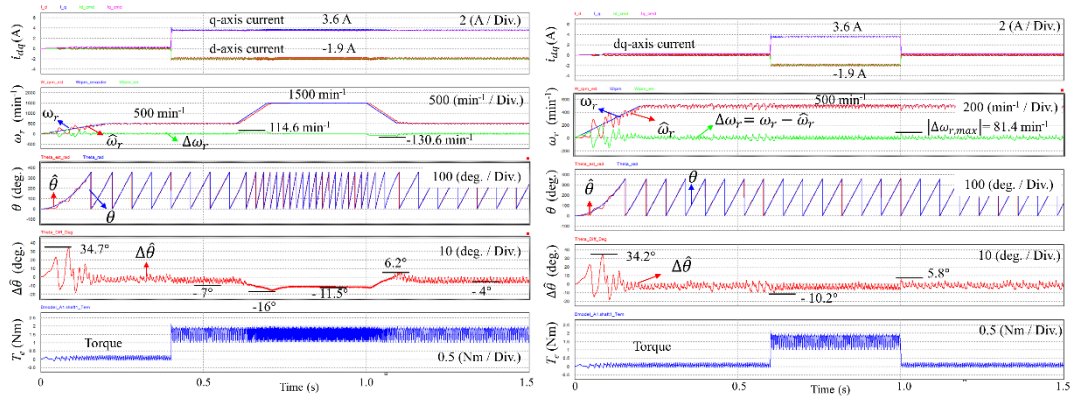

(a)(b)

Fig. 8: Simulation results on Double integral PLL-type estimator (a)Maximum overshoot in speed variation (b)Maximum overshoot in torque variation.

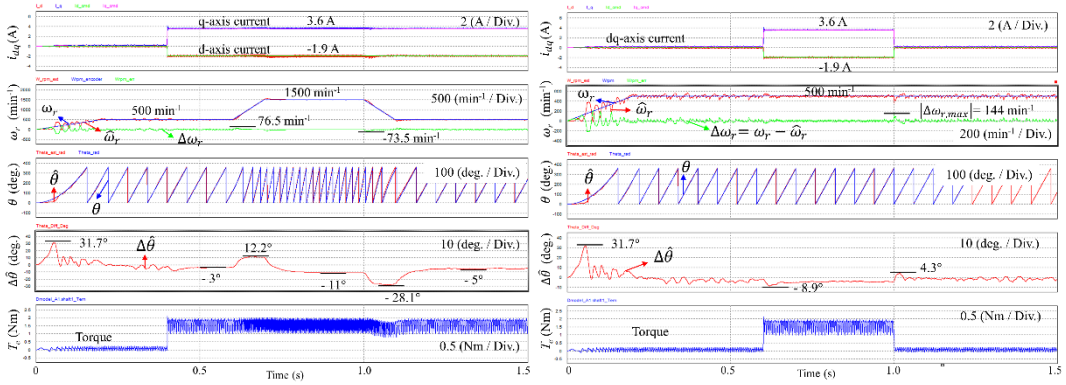

(a)(b)

Fig. 9: Simulation results on Luenberger Observer type estimator (a)Maximum overshoot in speed variation (b)Maximum overshoot in torque variation.

Table 2: Comparison result on speed and position estimators

Item	Step torque Max. $\Delta\omega_r$ [min^{-1}]	Rampwise speed Max. $\Delta\omega_r$ [min^{-1}]
PLL-type estimator	26.8	213.4
Double integral PLL-type estimator	81.4	-130.6
Luenberger Observer type estimator	144	76.5

The comparison results are shown in Table. 2. From this result, the maximum overshoot of PLL-type estimator is lower than other estimator methods in case of step torque response although the overshoot ofestimated speed error $\Delta\omega_r$ in rampwise speed variation is higher than other methods. Also, LO observer type estimator is lower than other estimator method in rampwise speed response. Therefore, to ensure optimal performance under transient conditions involving speed and torque fluctuations, the selection of an appropriate estimator for sensorless control must be carefully tailored to the specific dynamic and operational requirements of the target application.

6. Conclusion

This study analyzed the architecture and transient performance of various estimators used for speed and angle estimation in sensorless control of IPMSMs. Simulation results confirmed that instantaneous errors in the estimated speed and angle occur in response to rapid changes in speed and torque, and that the magnitude of these errors varies depending on the estimator type. Future research will evaluate the robustness of sensorless control by comparing estimator errors under motor parameter variations.

References

[1] P. Pillay and R. Krishnan, Application characteristics of permanent magnet synchronous and brushless dc motors for servo drives, *in Conf. Rec. IEEE-IAS Annu. Meeting, 3*, 2000, 1814-1819.

[2] S. Morimoto, K. Kawamoto, M. Sanada and Y. Takeda, Sensorless control strategy for salient-pole PMSM based on extended EMF in rotating reference frame, *IEEE Trans. Ind. Applicat., 38*, 2002, 1054-1061.

[3] H. Jang, S. K. Sul, J. I. Ha, K. Ide, and M. Sawamura, Sensorless drive of surface-mounted permanent-magnet motor by high-frequency signal injection based on magnetic saliency, *IEEE Trans. Ind. Appl., 39(4)*, 2003, 1031-1039.

[4] Lennart Harnefors and Hans-Peter Nee, A General Algorithm for Speed and Position Estimation of AC Motors, *IEEE Trans. Ind. Elec., 47(1)*, 2000, 77-83.

[5] Oskar Wallmark, Lennart Harnefors, and Ola Carlson, An Improved Speed and Position Estimator for Salient Permanent-Magnet Synchronous Motors, *IEEE Trans. Power Electron., 52(1)*, 2005, 255-262.

[6] Z. Q. Chen, M. Tomita, S. Doki, and S. Okuma, An extended electromotive force model for sensorless control of interior permanent magnet synchronous motors, *IEEE Trans. Ind. Electron., 50(2)*, 2003, 288-295.

[7] R. Bojoi, M. Pastorelli, J. Bottomley, P. Giangrande, C. Gerada, Sensorless control of PM motor drives — A technology status review, *IEEE Workshop on Electrical Machines Design Control and Diagnosis (WEMDCD)*, 2013, 168-182.

[8] H. Kim, M. C. Harke, and R. D. Lorenz, Sensorless control of interior permanent-magnet machine drives with zero-phase lag position estimation, *IEEE Trans. Ind. Appl.*, 2003, 1726-1733.

[9] G. C. Hsieh and J. C. Hung, Phase-locked loop techniques. A survey, *IEEE Trans. Ind. Electron., 43(6)*, 1996, 609-615.

[10] K. W. Lee, S. Park, and S. Jeong, A seamless transition control of sensorless PMSM compressor drives for improving efficiency based on a dual-mode operation,*IEEE Trans. Power Electron., 30(3)*, 2015, 1446-1456.

[11] Oskar Wallmark, and Lennart Harnefors, Sensorless Control of Salient PMSM Drives in the Transition Region, *IEEE Trans. Ind. Elec., 53(4)*, 2006, 1179-1187.

[12] R. W. Hejny, and R. D. Lorenz, Evaluating the practical low-speed limits for back-EMF tracking-based sensorless speed control using drive stiffness as a key metric, *IEEE Trans. on Ind. Appl., 47*, 2011, 1337-1343.

[13] H. Berriri, M. W. Naouar, and I. Slama-Belkhodja, Easy and fast sensor fault detection and isolation algorithm for electrical drives, *IEEE Trans. Power Electron., 27(2)*, 2012, 490-499.